Inorganic Chemistry

Article

pubs.acs.org/IC

Prebiotic NH_3 Formation: Insights from Simulations

András Stirling,*[,†] Tamás Rozgonyi,[‡] Matthias Krack,[§] and Marco Bernasconi[∥]

[†]Institute of Organic Chemistry, Research Centre for Natural Sciences of the Hungarian Academy of Sciences, POB 286, Budapest, 1519, Hungary

[‡]Institute of Materials and Environmental Chemistry, Research Centre for Natural Sciences of the Hungarian Academy of Sciences, POB 286, Budapest, 1519, Hungary

[§]Laboratory for Reactor Physics and Systems Behaviour, Paul Scherrer Institute, 5232 Villigen PSI, Switzerland

[∥]Department of Materials Science, University of Milano-Bicocca, Via R. Cozzi 55, Milano, Italy

Supporting Information

ABSTRACT: Simulations of prebiotic NH_3 synthesis from NO_3^- and NO_2^- on pyrite surfaces under hydrothermal conditions are reported. Ab initio metadynamics calculations have successfully explored the full reaction path which explains earlier experimental observations. We have found that the reaction mechanism can be constructed from stepwise single atom transfers which are compatible with the expected reaction time scales. The roles of the hot-pressurized water and of the pyrite surfaces have been addressed. The mechanistic picture that emerged from the simulations strengthens the theory of chemoautotrophic origin of life by providing plausible reaction pathways for the formation of ammonia within the iron−sulfur-world scenario.

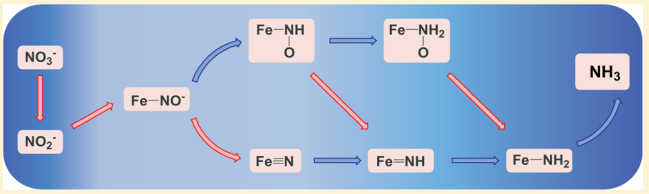

I. INTRODUCTION

According to the iron−sulfur world theory, life has begun as an autocatalytic surface metabolism of small organic molecules on minerals.[1,2] On an early Earth such scenario could operate in hydrothermal deep sea vents at high pressure and temperature. In this environment, iron-sulfide minerals are available abundantly providing conditions suitable for prebiotic redox processes.[3,4] The role of iron-sulfide minerals, and in particular pyrite in important prebiotic processes (e.g., synthesis of peptides or nucleic acid components) has been widely investigated and discussed, and the catalytic and support roles of the surfaces have been demonstrated.[2,5−13] An important constituent of the prebiotic pool of reactants is the most reduced nitrogen compound NH_3 which is a necessary precursor for nitrogen-containing organic molecules. Its formation from NO_x species (e.g., NO_2^- or NO_3^-) under assumed hydrothermal vent conditions has been already demonstrated in the presence of Fe^{2+} and on various iron-sulfides.[14−18] In particular, FeS has been used as reductant in refs 1d and 15−17, whereas FeS_2 was used in refs 15 and 18. The mechanism of the process leading to NH_3 is not only very significant from the perspective of prebiotic chemistry, but it can also provide important clues to interpret mineral surface reactivity and their oxidation in general.[19,20]

The current understanding of the reduction mechanism is still limited because of its complexity. The first attempt for the description of these processes at the molecular level has been provided by the calculation of adsorption energies and the assignments of IR spectra by means of small cluster models.[18] The decomposition of NO_2 and NO catalyzed by FeS_2 surfaces has also been studied theoretically because of its relevance in the acid mine drainage phenomenon; high dissociation barriers have been found indicating that molecular adsorption is preferred under normal conditions.[21] Still, a complete reaction mechanism is not available for the NH_3 formation. In order to achieve a detailed picture of the reaction mechanism more ambitious computational efforts are necessary. To this end we have performed an ab initio molecular dynamics (AIMD) study on large mineral−water interface models in combination with metadynamics to obtain information on the free energy surface (FES) of the elementary steps. Metadynamics[22] is a very efficient technique to explore and characterize reaction mechanisms by means of suitably chosen reaction coordinates.[23,24] In this work, we performed metadynamics simulations to uncover the mechanism of the $NO_3^- \rightarrow NH_3$ transformation on FeS_2 surfaces. In particular we address the role of the mineral surface and of hydrothermal conditions in this primordial heterogeneous key reaction. Although the reaction steps leading to the formation of ammonia are not known, various scenarios for pyrite oxidation are possible and all indicate a very high (98−173 kcal/mol) reaction enthalpy driving the ammonia formation.[25] The extreme conditions may trigger a multitude of reactions and side reactions which would require enormous computational efforts to be fully explored. Therefore, we here aim at finding possible reaction paths leading to NH_3 formation rather than attempting to explore the

Received: December 16, 2015
Published: February 2, 2016

DOI: 10.1021/acs.inorgchem.5b02911
Inorg. Chem. 2016, 55, 1934−1939

whole reaction space defined by our reactants (NO_x^- ions, pyrite, and water).

II. COMPUTATIONAL DETAILS

A. Quantum Chemical Calculations. Born−Oppenheimer molecular dynamics simulations based on density functional theory have been performed using the Quickstep module of the CP2K program suite.[26] The Perdew−Becke−Ernzerhof (PBE) exchange and correlation functional has been used.[27] The GTH-type pseudopotentials have been employed to describe the interaction between the valence electrons and the ionic cores.[28] The short-range, molecularly optimized MOLOPT-SR double-ζ basis sets have been used to expand the valence orbitals.[29] For the S, O, N, and H atoms the basis was augmented by a set of polarization functions (DZVP). An auxiliary basis set of plane waves with a kinetic energy cutoff of 400 Ry has been employed to expand the electronic charge density. Only the Γ-point has been considered for the *k*-point sampling. The present setup gives a nonmagnetic ground state. The calculations have been performed in restricted Kohn−Sham formalism assuming closed shell states. Empirical dispersion corrections[30] have not been included into the Hamiltonian. While they can be very important when long-range interactions play an important role, in our systems the reactive events are localized; therefore, we do not expect large improvements from disperion corrections.[31] Our methodology yields an optimal cell constant of 5.417 Å with a 96-atom bulk pyrite supercell which agrees nicely with experiment (e.g., 5.416 Å,[32] 5.428 Å[33]). The estimated band gap is 0.4 eV (experimental value[34] is 0.95 eV). This underestimation is typical for functionals applying only standard semilocal approximations[35] but in the light of earlier evidence[11,12,36−38] we do not expect that this feature affects the main conclusions. The charge state of the intermediates has been determined by analyzing the maximally localized Wannier functions of the Kohn−Sham orbitals.[31,39]

B. Model Construction. In this study we employ the same large pyrite−water interface models which have been employed in our previous study.[40] The pyrite−water interface has been modeled by a pyrite slab of 12 pyrite layers (Figure 1). Each layer is composed of eight iron or sulfur atoms; that is, they represent a 2 × 2 surface supercell. The bottom of the slab has been saturated by water molecules attached to the surface iron atoms. This termination has been shown to provide bulk-like electronic configuration for the iron surface atoms.[36] The three bottom pyrite layers and the O atoms of the terminating H_2O molecules are kept fixed during all the simulations. Two configurations of the (100) surface have been considered: the ideal configuration with no defects which was shown not to reconstruct in previous works and a configuration with a sulfur vacancy. This has been created by removing a top sulfur atom from the perfect surface. The sulfur vacancy is known to be one of the most frequent surface defects on pyrite.[41] The size of the periodic simulation cells is 10.8348 × 10.8348 × 26.8348 $Å^3$. The slabs are separated by ∼14 Å distance and this space is filled up with water molecules The supercritical conditions have been modeled by setting the temperature to 800 K and the density of the water layer to 0.5 g/cm^3 with 28 water molecules which is equivalent to 0.1 GPa according to the water equation of state.[42] We note that the volume available between the two pyrite layers is not well-defined therefore the density and the corresponding pressure is only approximately determined by the number of the H_2O molecules.

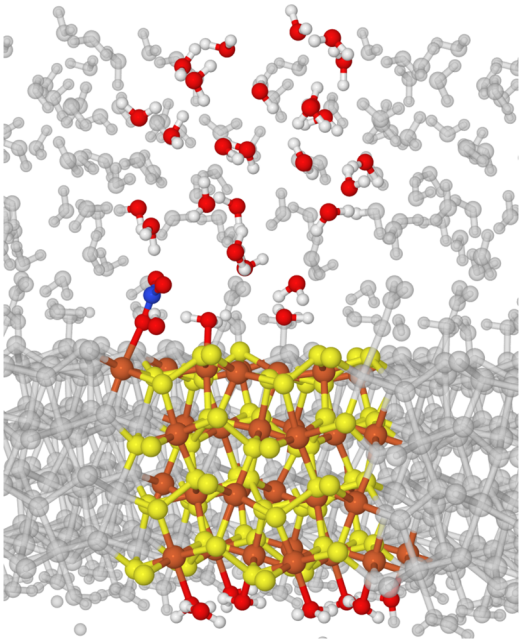

Figure 1. Model of the pyrite−water interface with a NO_3^- anion embedded into its periodic images used in the simulations. The simulation cell is colored, the periodic images are translucent gray. Color code: brown: Fe; yellow: S; red: O; blue: N; white: H.

C. MD Simulations. For this study we have selected the conditions from ref 15 (800 K, 0.1 GPa), because in this case the NH_3 production was more than 70%, while milder conditions led to very limited NH_3 yield (∼5%).[18,43] The MD simulations have been performed under NVT conditions employing the velocity rescaling thermostat of Bussi et al.[44] The coupling time constant of the thermostat has been set to 1 ps for the equilibration and 80 fs for the metadynamics. The time step for integrating the Verlet equations of the MD was 0.4 fs. This was sufficiently small to obtain a stable integration around the target temperature of 800 K. The water-pyrite interfaces have been equilibrated for ∼40 ps. Then a NO_3^- or a NO_2^- ion has been inserted into the water layer in the vicinity of the surface and a ∼ 10 ps equilibration has been performed. In the Quickstep code the negative charge is compensated by a uniform positive countercharge in order to have neutral periodic images.

During the equilibration of the system containing a NO_3^- ion and defect-free FeS_2 surface a harmonic wall potential was applied to keep the nitrate ion in the vicinity of the surface (within 3.6 Å layer from the surface iron atoms). The force constant of the quadratic wall potential switched on if the nitrate leaves this region was set to 1.0 Ha/$bohr^2$.

The free energy barriers have been obtained by applying the metadynamics technique.[22,45] Metadynamics is a highly efficient technique to sample the FES of rare events as a function of a few selected reaction coordinates (collective variables, CVs). It has been employed successfully in various fields,[46] and its various aspects have been reviewed recently.[23,24,47] Several functions of the relevant bond distances have been considered to describe the O transfers between the NO_x^- species and the pyrite surface, and the H transfers from the water molecules to N. We have selected various functions of coordination numbers[48] (CNs) as CVs. CNs are functions of the nuclear coordinates as shown in eqs 1 and 2. A CN between a single atom (A) and a group of atoms ({B}) can be written as

$$\mathrm{CN}_{\mathrm{A}-\{\mathrm{B}\}} = \sum_{i\in\{\mathrm{B}_i\}} \frac{1-\left(\frac{r_i}{r_c}\right)^p}{1-\left(\frac{r_i}{r_c}\right)^q} \tag{1}$$

where r_i is the distance of atom A from the *i*th B atom, and r_c is a cutoff distance related to the bond distance between A and B. CN can also be defined conveniently between two groups of atoms ({A} and {B}):

$$\mathrm{CN}_{\{\mathrm{A}\}-\{\mathrm{B}\}} = \sum_{i\in\{\mathrm{A}\}/j\in\{\mathrm{B}\}} \frac{1-\left(\frac{r_{ij}}{r_c}\right)^p}{1-\left(\frac{r_{ij}}{r_c}\right)^q} \tag{2}$$

where r_{ij} is the distance between two atoms of the two groups and r_c is again a suitable cutoff distance. *p* and *q* are integer parameters. The above CNs provide an easy way to follow the chemical changes in the system: they count the number of the bonds between the selected

DOI: 10.1021/acs.inorgchem.5b02911
Inorg. Chem. 2016, 55, 1934−1939

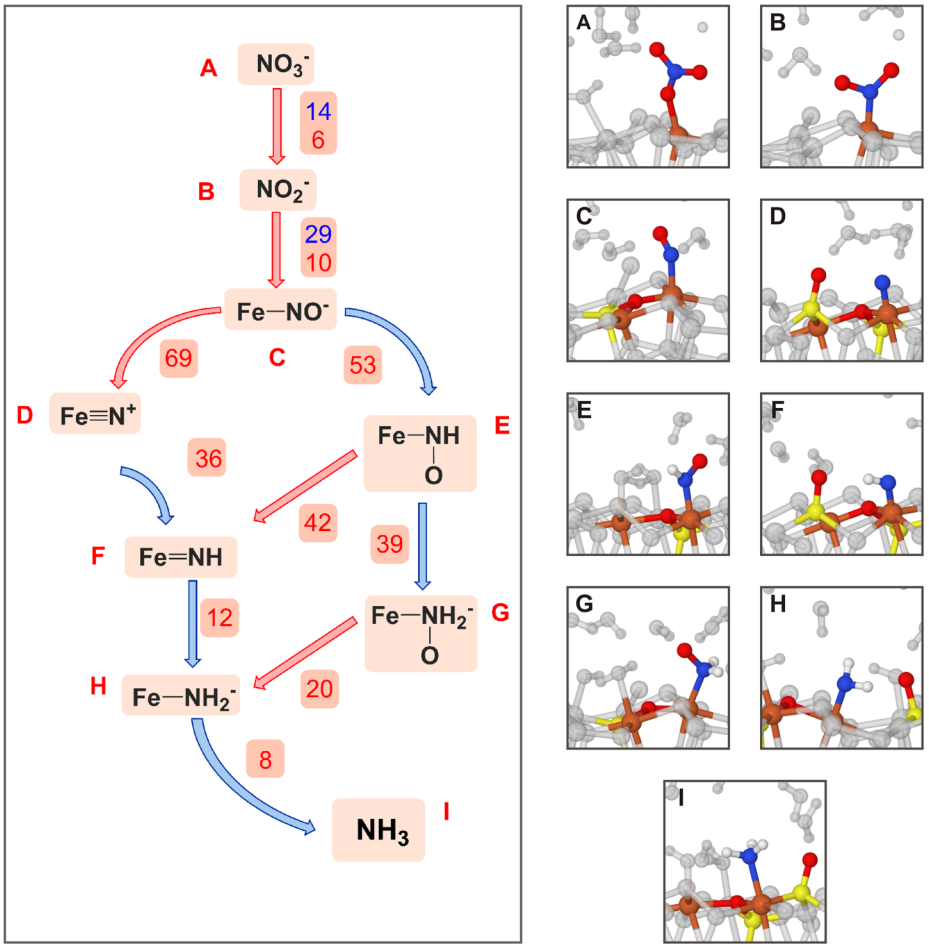

Figure 2. Left panel: The reaction pathways emerged from the metadynamics simulations. Letters (A–I) label the reactions steps. Red arrows indicate oxygen transfers, while blue arrows indicate hydrogen transfers. Charge states are determined from the distribution of the centers of the maximally localized Wannier functions.[31] The activation free energies of the steps are also shown (in kcal/mol). Blue values refer to barriers obtained on perfect pyrite surface, whereas red values correspond to the defective surface. Note that starting from stage C the defective site is filled by an O atom. The adsorbed species form bond with an iron (Fe) atom. Right panels: Representative snapshots of the reactant, intermediate and product species on the defective surface. For color code see Figure 1.

atoms and any change (bond breaking or bond formation) yields an approximately unit change in their value. The selected CVs and their chemical roles together with further technical details of the metadynamics simulations are given in the Supporting Information (SI).

III. RESULTS

In an earlier study we scrutinized the water-pyrite interface under hydrothermal conditions.[40] It was shown that at these extreme conditions the pyrite surface is hardly covered by water. This results in fully exposed surface atoms and a reactivity which does not require prior water desorption.[49] This particular mineral-water interface accommodates the reaction steps leading to the $NO_x^- \rightarrow NH_3$ transformation. In Figure 2 the reaction pathways emerged from the simulations are shown with the free energy barriers of the forward steps. Representative snapshots of reaction intermediates are also shown in Figure 2 while snapshots of the transition states are collected in the SI. The barriers are compatible with the reaction time scale measured experimentally (e.g., 24 h at supercritical conditions).[15,18,50] The simulations have revealed that the $NO_3^- \rightarrow NH_3$ transformation proceeds via consecutive single atom (either O or H) transfers. Reaction steps where two or more atoms are transferred concertedly have not been observed. It is important to note here that the CVs of the simulations allowed both single and concerted multiatom transfers and metadynamics selected the path where the free energy barrier is smaller.

The full reduction path is started by the stepwise oxygen atom transfers from NO_3^- to the pyrite surface. In these steps it was sufficient to employ CVs which describe the bonding of these O atoms: a coordination number (CN) describing bond formation between any of the oxygen atoms in the NO_x^- species (x = 3 or 2) and the Fe or S atoms on the pyrite surface and another CN boosting the cleavage of any of the N–O bonds.[31,51] MD simulations showed that the NO_3^- anion adsorbs very weakly on the perfect FeS_2 surface but the presence of a defect site strongly enhances its adsorption on the undercoordinated Fe atoms close to the vacancy.[31] All the other N-species adsorb strongly on the surface Fe atoms in all cases at the simulation time-scales. The weak affinity of the nitrate anion toward the FeS_2 surface can be explained by recalling that NO_3^- is a particularly weakly coordinating anion as opposed to other NO_x species.[52]

During the first step NO_3^- adsorbs on the perfect surface in monodentate mode (see Figure 2A and in Figure S4 in SI), then the N–O bond breaks leaving an O atom bound to the Fe

DOI: 10.1021/acs.inorgchem.5b02911
Inorg. Chem. 2016, 55, 1934–1939

atom and the NO_2^- anion diffusing back into the water. On the defective surface, the O transfer takes place in a temporary bidentate mode to a defective iron atom (Figure S5) and then the NO_2^- desorbs. The products of the subsequent decompositions of NO_2^- remain instead all bound to the surface. Desorption implies that reduction of NO_2^- occurs more likely at a different site not yet oxidized by NO_3^-. However, the steps following the reduction of NO_2^- all take place at the same site because of the formation of a strong N−Fe bond. The first and second O atoms remain on surface iron atoms after the N−O bond breaking. Analysis of the charges showed that during these transfers formally a neutral O atom migrated. Note that transfer of a neutral O atom represents a 2e reduction of nitrogen and a 2e oxidation of the surface atom binding this O atom. The calculations have shown that when a sulfur vacancy is present, both reduction steps are kinetically more favorable as indicated by significantly smaller activation free energies and the dissociating O atom fills in the defect site. Earlier calculations[8,11,12,38,40,53] as well as experiments[19,20] have also convincingly showed that vacancies are very reactive and favor redox processes.

We have simulated both the $NO_3^- \rightarrow NO_2^-$ and the $NO_2^- \rightarrow NO^-$ reactions in the presence of an empty S vacancy that is filled by the O atom transferred to the surface. The subsequent reaction steps (from C to I in Figure 2) on the defective surface have been simulated in the presence of a sulfur vacancy filled by an oxygen atom at step C. The extreme conditions have a remarkable acceleration effect on these steps. Indeed, nudged elastic band (NEB) calculations (without water and at 0 K) predict much slower reaction steps in vacuum.[54] The increasing free energy barriers of the O-transfers verify a posteriori our assumption that surface defects can be easily consumed during the initial stage of the process and they cannot play a major role later.

Many reaction paths are conceivable for the conversion of nitrosyl species. We have addressed this problem by using CVs which also involve water participation. Such CVs are the CN between the nitrogen atom and the hydrogen atoms of the water layer, the CNs between the water oxygen and hydrogen atoms and a CN between the water oxygens and the surface iron and sulfur atoms. Appropriate functions of these CVs have been employed to describe the combined effect of the surface water interface.[31] We have found that the barrier to transfer the last oxygen atom to the surface depends largely on the number of hydrogen atoms bonded to N. Direct formation of a nitride species (step C → D in Figure 2) requires a barrier of 69 kcal/mol. Analysis of the charge distribution[31] showed that this species is analogous to the recently discovered Fe(VI)−nitrido complex.[55,56] This intermediate is highly reactive and we indeed observed that it could rapidly build into the lattice when other reaction did not consume it. In contrast, when an oxygen atom transfer takes place in the presence of one or two H atoms in the molecule, the free energy barriers are 42 (step E → F) and 20 kcal/mol (step G → H), respectively. The high barrier of the nitride formation indicates that this step can be excluded from the mechanism. Interestingly the stepwise protonation also features a decreasing trend in the barriers: along the $NO_x \rightarrow NHO_x \rightarrow NH_2O_x$ path (x = 1 or 0) the free energy barriers always decrease remarkably, even if oxygen loss occurs concurrently. In agreement with earlier findings,[53] the last O atom is transferred to a neighbor S atom in all cases as seen in Figure 2. The final step for NH_3 formation requires a barrier of only 8 kcal/mol indicating a very fast step at hydrothermal conditions. The NH_3 formed in the last step is initially adsorbed on an iron site but it desorbs after a few hundreds of fs. Figure 3 shows the FES of a reaction path following the sequence NO−NHO−NH−NH_2−NH_3. The free energy wells can be easily associated with the corresponding intermediate states. In Figure 4 the temporal variations of the individual CVs of the same run are plotted. The surface coverage by water is also plotted to illustrate that at the simulation conditions the surface remains dry.

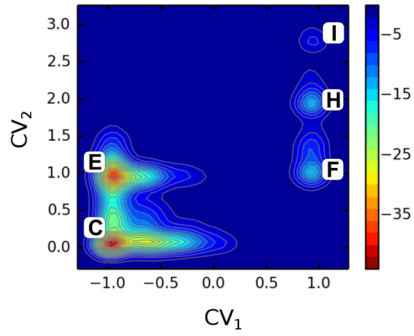

Figure 3. Contour plot of the FES (kcal/mol) characterizing a typical $NO^- \rightarrow NH_3$ transformation along the NO−NHO−NH−NH_2−NH_3 path. The labels indicate the reaction intermediates according to Figure 2. CV_1 is the difference of CN between the O atom with the surface atoms and the CN between the same O atom and the N atom. The value of CV_1 increases by ∼1 if the N−O bond breaks and also when the O atom forms a bond with any surface atom. CV_2 is the CN between the N atom and all the H atoms of the system. Its value increases by ∼1 when a N−H bond is formed.

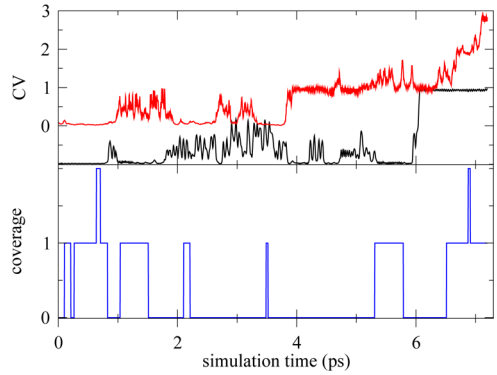

Figure 4. Top: Temporal variation of CV_1 (black) and CV_2 (red) in the simulation of Figure 3. Bottom: Variation of the surface water coverage (number of adsorbed H_2O) in the same simulation (the number of available iron sites for adsorption is 7). A water molecule is adsorbed when the water−iron distance is below 2.9 Å. For an explanation of the CVs see Figure 3.

As Figure 2 shows the Fe-NHO state is also a bifurcation point: a proton transfer from water to N (E → F) and the O loss (E → G) have very similar (42 and 39 kcal/mol) activation barriers. Then the further steps have lower barriers indicating that the kinetic bottleneck is the formation of the Fe-NHO state (as nitride formation is excluded from the mechanism). This result also implies that the preceding nitrosyl species can be the most likely candidate among the intermediates to be captured experimentally. Strongin et al. have indeed detected such species by ATR-FTIR method but under much milder conditions.[18]

DOI: 10.1021/acs.inorgchem.5b02911
Inorg. Chem. 2016, 55, 1934−1939

In most of the cases the proton is transferred from a water molecule adsorbed in a neighbor iron site (see Figures S5: G, H and J in the SI) although we also observed proton transfer from the water phase (e.g., Figure S5: E) or formation of a proton wire (e.g., Figure S5: D). In these cases the surface has an important role in promoting the reactions by confining the reactants into close vicinity. However, we note that adsorption and desorption were quite frequent events (albeit short, a few hundreds fs at most) in the simulation time scale and specifically biasing water adsorption for proton transfer has not reduced the barriers involving H-transfers.[31]

Finally it is an important issue to take account of the 8 electrons transferred along the reduction path $NO_3^- \rightarrow NH_3$. The 3 O atom transfers leave 6 e on the nitrogen, and consequently, they result in a significant oxidation of the surface Fe and S sites, where they bind. The remaining 2 e come directly from the surface, namely from a nearby Fe site. Inspection of the Wannier centers shows considerable fluctuations at the simulation conditions. This facilitates redox processes between the different surface sites. Indeed we found that the second proton uptake is accompanied by a 2e transfer to the iron site binding the NHO_x (x = 0 or 1) unit, which are then transferred to the N atom.

IV. CONCLUSIONS

Overall the simulations suggest the following mechanistic picture in agreement with earlier experiments.[15] The $NO_3^- \rightarrow NH_3$ transformation can occur on a FeS_2 (100) surface in a stepwise single-atom transfer fashion. This process starts preferably on defect sites. The kinetic bottleneck of the full process is the reduction of NO^- bound to an iron surface site. Two quasiequivalent paths operate simultaneously from the NHO species (E−F−H−I and E−G−H−I). We note that these reaction intermediates show striking analogy to those identified in the mechanism of nitrite reductase enzyme.[57] Water participates in the processes as reactant and as an environment supplying the thermodynamic conditions which have a significant acceleration effect on the reactions. The role of pyrite in the process is 2-fold: it is a reactant and a support. It is a reactant by abstracting oxygen atoms stepwise. Its support role is to bind the N-containing species on the surface during the reactions, which allows for a simultaneous contact with water and the surface atoms for oxygen atom and proton transfers. The extreme conditions provide a particularly suitable interface arrangement[40] for this 2-fold role because the accessible surface sites are not covered by water thus providing room for both the adsorption and the reduction. Our model provides a plausible mechanistic picture of how NH_3 can form in hydrothermal vents which may have operated on the early Earth in the synthesis of prebiotic molecules. As ammonia is an essential prebiotic reactant, the present mechanistic picture provides further support for the role of iron sulfide minerals in the chemoautotrophic origin of life.

■ ASSOCIATED CONTENT

Supporting Information

The Supporting Information is available free of charge on the ACS Publications website at DOI: 10.1021/acs.inorgchem.5b02911.

The details of the NEB computations and ab initio MD simulations, the Wannier localization of the Kohn−Sham orbitals, the description of the CVs employed in the study, a discussion on the error sources, representative TS configurations and the FES-s of the most important reaction paths. (PDF)

■ AUTHOR INFORMATION

Corresponding Author

*E-mail: stirling.andras@ttk.mta.hu.

Notes

The authors declare no competing financial interest.

■ ACKNOWLEDGMENTS

Support of OTKA Grant K101115 is acknowledged. This work was supported by a grant from the Swiss National Supercomputing Centre (CSCS) under project ID s427. Support of Hungarian National Development Agency grant KTIA_AIK_12-1-2012-0014 and computational resources provided by NIIF Supercomputer Center are also acknowledged The authors are indebted to Prof. Michele Parrinello for his suggestions and ideas at the beginning of this project.

■ REFERENCES

(1) (a) Wächtershäuser, G. *Microbiol. Rev.* **1988**, *52*, 452−484. (b) Wächtershäuser, G. *Prog. Biophys. Mol. Biol.* **1992**, *58*, 85−201. (c) Drobner, E.; Huber, H.; Wächtershäuser, G.; Rose, D.; Stetter, K. O. *Nature* **1990**, *346*, 742−744. (d) Blöchl, E.; Keller, M.; Wächtershäuser, G.; Stetter, O. K. *Proc. Natl. Acad. Sci. U. S. A.* **1992**, *89*, 8117. 1992

(2) Ruiz-Mirazo, K.; Briones, C.; de la Escosura, A. *Chem. Rev.* **2014**, *114*, 285−366.

(3) Holm, N. G. *Origins Life Evol. Biospheres* **1992**, *22*, 5−14.

(4) Yücel, M.; Gartman, A.; Chan, C. S.; Luther, G. W., III *Nat. Geosci.* **2011**, *4*, 367−371.

(5) McGuinness, E. T. *Chem. Rev.* **2010**, *110*, 5191−5215.

(6) Boehme, C.; Marx, D. *J. Am. Chem. Soc.* **2003**, *125*, 13362−13363.

(7) Schoonen, M.; Smirnov, A.; Cohn, C. *Ambio* **2004**, *33*, 539−551.

(8) Nair, N. N.; Schreiner, E.; Marx, D. *J. Am. Chem. Soc.* **2006**, *128*, 13815−13826.

(9) Pollet, R.; Boehme, C.; Marx, D. *Origins Life Evol. Biospheres* **2006**, *36*, 363−379.

(10) Saladino, R.; Neri, V.; Crestini, C.; Costanzo, G.; Graciotti, M.; Di Mauro, E. *J. Am. Chem. Soc.* **2008**, *130*, 15512−15518.

(11) Schreiner, E.; Nair, N. N.; Marx, D. *J. Am. Chem. Soc.* **2008**, *130*, 2768−2770.

(12) Schreiner, E.; Nair, N. N.; Wittekindt, C.; Marx, D. *J. Am. Chem. Soc.* **2011**, *133*, 8216−8226.

(13) Roldan, A.; Hollingsworth, N.; Roffey, A.; Islam, H. U.; Goodall, J.; Catlow, C. R. A.; Darr, J. A.; Bras, W.; Sankar, G.; Holt, K. B.; Hogarth, G.; de Leeuw, N. H. *Chem. Commun.* **2015**, *51*, 7501−7504.

(14) Summers, D. P.; Chang, S. *Nature* **1993**, *365*, 630−633.

(15) Brandes, J. A.; Boctor, N. Z.; Cody, G. D.; Cooper, B. A.; Hazen, R. M.; Yoder, H. S. J. *Nature* **1998**, *395*, 365−367.

(16) Dörr, M.; Käßbohrer, J.; Grunert, R.; Kreisel, G.; Brand, W. A.; Werner, R. A.; Geilmann, H.; Apfel, C.; Robl, C.; Weigand, W. *Angew. Chem., Int. Ed.* **2003**, *42*, 1540−1543.

(17) Summers, D. P. *Origins Life Evol. Biospheres* **2005**, *35*, 299−312.

(18) Singireddy, S.; Gordon, A. D.; Smirnov, A.; Vance, M. A.; Schoonen, M. A. A.; Szilagyi, R. K.; Strongin, D. R. *Origins Life Evol. Biospheres* **2012**, *42*, 275−294.

(19) Rosso, K. M.; Vaughan, D. J. *Rev. Mineral. Geochem.* **2006**, *61*, 557−607.

(20) Murphy, R.; Strongin, D. R. *Surf. Sci. Rep.* **2009**, *64*, 1−45.

(21) Sacchi, M.; Galbraith, M. C. E.; Jenkins, S. J. *Phys. Chem. Chem. Phys.* **2012**, *14*, 3627−3633.

DOI: 10.1021/acs.inorgchem.5b02911
Inorg. Chem. 2016, 55, 1934−1939

(22) (a) Laio, A.; Parrinello, M. *Proc. Natl. Acad. Sci. U. S. A.* **2002**, *99*, 12562−12566. (b) Iannuzzi, M.; Laio, A.; Parrinello, M. *Phys. Rev. Lett.* **2003**, *90*, 238302.
(23) Barducci, A.; Bonomi, M.; Parrinello, M. *Wiley Interdiscip. Rev.: Comput. Mol. Sci.* **2011**, *1*, 826−843.
(24) Stirling, A.; Nair, N. N.; Lledós, A.; Ujaque, G. *Chem. Soc. Rev.* **2014**, *43*, 4940−4952.
(25) Standard reaction enthalpies referenced to one mole of FeS_2 for the following reactions

$$4FeS_2 + 5NO^-_{3(aq)} + 11H_{2O} = 4Fe^{2+}_{(aq)} + 8SO^{2-}_{3(aq)} + 5NH^+_{4(aq)} + 2OH^-_{(aq)}$$

$$8FeS_2 + 11NO^-_{3(aq)} + 18H_2O = 8Fe^{3+}_{(aq)} + 16SO^{2-}_{3(aq)} + 11NH_{3(aq)} + 3OH^-_{(aq)}$$

$$4FeS_2 + 7NO^-_{3(aq)} + 17H_{2O} = 4Fe^{2+}_{(aq)} + 8SO^{2-}_{4(aq)} + 7NH^+_{4(aq)} + 6OH^-_{(aq)}$$

$$8FeS_2 + 15NO^-_{3(aq)} + 26H_{2O} = 8Fe^{3+}_{(aq)} + 16SO^{2-}_{4(aq)} + 15NH_{3(aq)} + 7OH^-_{(aq)}$$

are −99.7, −97.9, 174.1, and 172.7 kcal/mol, respectively. Standard enthalpies of formations are from *CRC Handbook of Chemistry and Physics*; Weast, R. C., Lide, D. R., Astle, M. J., Beyer, W. H., 70th ed., CRC Press: Boca Raton, FL, 1990.
(26) The CP2K Developers Group. Available at: www.cp2k.org;. VandeVondele, J.; Krack, M.; Mohamed, F.; Parrinello, M.; Chassaing, T.; Hutter, J. *Comput. Phys. Commun.* **2005**, *167*, 103−128.
(27) Perdew, J. P.; Burke, K.; Ernzerhof, M. *Phys. Rev. Lett.* **1996**, *77*, 3865−3868.
(28) Goedecker, S.; Teter, M.; Hutter, J. *Phys. Rev. B: Condens. Matter Mater. Phys.* **1996**, *54*, 1703−1710. Krack, M. *Theor. Chem. Acc.* **2005**, *114*, 145−152.
(29) VandeVondele, J.; Hutter, J. *J. Chem. Phys.* **2007**, *127*, 114105.
(30) Grimme, S. *WIREs Comput. Mol. Sci.* **2011**, *1*, 211−228.
(31) Further details can be found in the SI.
(32) Stevens, E. D.; DeLucia, M. L.; Coppens, P. *Inorg. Chem.* **1980**, *19*, 813−820.
(33) Finklea, S. L.; Cathey, L.; Amma, L. *Acta Crystallogr., Sect. A: Cryst. Phys., Diffr., Theor. Gen. Crystallogr.* **1976**, *32*, 529−537.
(34) Ennaoui, A.; Fiechter, S.; Pettenkofer, C.; Alonso-Vante, N.; Büker, K.; Bronold, M.; Höpfner, C.; Tributsch, H. *Sol. Energy Mater. Sol. Cells* **1993**, *29*, 289−370.
(35) Perdew, J. P.; Parr, R. G.; Levy, M.; Balduz, J. L. *Phys. Rev. Lett.* **1982**, *49*, 1691−1694.
(36) Stirling, A.; Bernasconi, M.; Parrinello, M. *J. Chem. Phys.* **2003**, *118*, 8917−8926.
(37) Stirling, A.; Bernasconi, M.; Parrinello, M. *J. Chem. Phys.* **2003**, *119*, 4934−4939.
(38) Stirling, A.; Bernasconi, M.; Parrinello, M. *Phys. Rev. B: Condens. Matter Mater. Phys.* **2007**, *75*, 165406.
(39) Marzari, N.; Mostofi, A. A.; Yates, J. R.; Souza, I.; Vanderbilt, D. *Rev. Mod. Phys.* **2012**, *84*, 1419−1475.
(40) Stirling, A.; Rozgonyi, T.; Krack, M.; Bernasconi, M. *Phys. Chem. Chem. Phys.* **2015**, *17*, 17375−17379.
(41) Rosso, K. M.; Vaughan, D. J. *Rev. Mineral. Geochem.* **2006**, *61*, 505−556.
(42) Saul, A.; Wagner, W. *J. Phys. Chem. Ref. Data* **1989**, *18*, 1537−1564.
(43) The experiment[15] we are reproducing has been conducted in the following manner: FeS_2 was prepared from pure metal and elemental sulphur. An aqueous solution of NO_3^- or NO_2^- was reacted with FeS_2 in N_2-purged, acid-washed gold tube, which was welded shut and incubated, and after 24 h it was opened, extracted with water, and analyzed for NO_x^- and NH_3 species,by spectroscopic methods.
(44) Bussi, G.; Donadio, D.; Parrinello, M. *J. Chem. Phys.* **2007**, *126*, 014101.
(45) Laio, A.; Rodriguez-Fortea, A.; Gervasio, F. L.; Ceccarelli, M.; Parrinello, M. *J. Phys. Chem. B* **2005**, *109*, 6714.
(46) See for example. (a) Ensing, B.; Laio, A.; Gervasio, F. L.; Parrinello, M.; Klein, M. *J. Am. Chem. Soc.* **2004**, *126*, 9492. (b) Comas-Vives, A.; Stirling, A.; Lledós, A.; Ujaque, G. *Chem. - Eur. J.* **2010**, *16*, 8738−8747. (c) Stanton, C. L.; Kuo, I.-F. W.; Mundy, C. J.; Laino, T.; Houk, K. N. *J. Phys. Chem. B* **2007**, *111*, 12573. (d) Stirling, A.; Pápai, I. *J. Phys. Chem. B* **2010**, *114*, 16854−16859. (e) Cavalli, A.; Spitaleri, A.; Saladino, G.; Gervasio, F. L. *Acc. Chem. Res.* **2015**, *48*, 277−285.
(47) (a) Laio, A.; Parrinello, M. *Lect. Not. Phys.* **2006**, *703*, 315. (b) Laio, A.; Gervasio, F. L. *Rep. Prog. Phys.* **2008**, *71*, 126601.
(48) Sprik, M. *Faraday Discuss.* **1998**, *110*, 437.
(49) Strong desoprtion tendency has been observed earlier also; see, e.g., ref 9.
(50) The activation free energy of typical reactions taking place in solution within a few hours at ambient conditions is 15−20 kcal/mol. This energy range is equivalent to about 25−42 k_BT at 298 K. At 800 K the same interval corresponds to the activation barrier range of 40−67 kcal/mol.
(51) CVs involving water participation in the reactions did not change the mechanism:at first O transfers take place.
(52) Rasmussen, S. C. *ChemText* **2015**, *1*, 1−10.
(53) Rozgonyi, T.; Stirling, A. *J. Phys. Chem. C* **2015**, *119*, 7704−7710.
(54) NEB calculations have been performed to simulate the reduction without water. See the details in the SI.
(55) Berry, J. F.; Bill, E.; Bothe, E.; George, S. D.; Mienert, B.; Neese, F.; Wieghardt, K. *Science* **2006**, *312*, 1937−1941.
(56) Hohenberger, J.; Ray, K.; Meyer, K. *Nat. Commun.* **2012**, *3*, 720.
(57) Bykov, D.; Neese, F. *Inorg. Chem.* **2015**, *54*, 9303−9316.

DOI: 10.1021/acs.inorgchem.5b02911
Inorg. Chem. 2016, 55, 1934−1939